Journal of Catalysis 349 (2017) 136–148

Contents lists available at ScienceDirect

Journal of Catalysis

journal homepage: www.elsevier.com/locate/jcat

Benzene co-reaction with methanol and dimethyl ether over zeolite and zeotype catalysts: Evidence of parallel reaction paths to toluene and diphenylmethane

Juan S. Martinez-Espin [a,b], Kristof De Wispelaere [c], Marius Westgård Erichsen [a], Stian Svelle [a], Ton V.W. Janssens [b], Veronique Van Speybroeck [c,*], Pablo Beato [b,*], Unni Olsbye [a,*]

[a] Centre for Materials Science and Nanotechnology, Department of Chemistry, University of Oslo, P.O. Box 1033, Blindern, N-0315 Oslo, Norway
[b] Haldor Topsøe A/S, Haldor Topsøes Allé 1, DK-2800 Kgs. Lyngby, Denmark
[c] Center for Molecular Modeling, Ghent University, Technologiepark 903, B-9052 Zwijnaarde, Belgium

ARTICLE INFO

Article history:
Received 18 September 2016
Revised 20 February 2017
Accepted 7 March 2017

Keywords:
Benzene
Methanol
Dimethyl ether
Methylation
Zeolites
Methanol-to-hydrocarbons
Diphenylmethane
Formaldehyde

ABSTRACT

The reactivity of methanol (MeOH) and dimethyl ether (DME) toward benzene was studied over zeolitic materials with different topology and acid strength (H-ZSM-5, H-SSZ-24, and H-SAPO-5) at 250–350 °C. Higher rates of methylation, and subsequent de-alkylation reactions, were observed with DME compared to MeOH. In addition, significant differences in product distribution based on the choice of methylating agent were observed. For reactions between MeOH and benzene a fraction of diphenylmethanes (DPMs) was formed, while this product group was nearly absent during reactions between DME and benzene. A range of co-feed and isotopic labeling experiments was performed, mainly over H-ZSM-5, in order to elucidate mechanistic information on the pathway from methanol and benzene to DPMs. Overall, these studies revealed that DPM formation involves the dehydrogenation of methanol to formaldehyde on the Brønsted acid site, followed by subsequent reaction with two benzene molecules. Theoretical calculations confirmed the higher reactivity of DME compared to MeOH toward benzene methylation and suggested a plausible route from formaldehyde and benzene to DPM.

1. Introduction

Zeolite-catalyzed methylation reactions are important in a number of large scale petrochemical industrial processes such as xylene and 2,6-dimethylnapthalene production [1,2]. Methylation reactions are also key steps in the increasingly relevant Methanol-To-Hydrocarbons (MTH) reaction, which include the Methanol-To-Gasoline (MTG), Methanol-To-Olefins (MTO) and Methanol-To-Propene (MTP) processes [3–6].

Zeolitic catalysts provide suitable environments for shape selective catalytic hydrocarbon transformations and methylations due to their large surface areas, strong Brønsted acidity and pore systems of molecular dimensions [7–10], which can be exploited to control the product distribution. Recent studies of the MTH reaction over micron-sized H-ZSM-5 crystals and 2–4 nm thick H-ZSM-5 nanosheets revealed that the product distribution is mainly maintained when diffusional constraints are eliminated [11,12], indicating that the confinement in zeolite pores dominates the observed product distribution of the MTH reaction in H-ZSM-5.

Hydrocarbon methylation over zeolitic catalysts has been the topic of numerous fundamental studies over the past decades. These studies have aimed at disclosing the effect of hydrocarbon size and class, zeolite topology, acid strength and active site environment on the intrinsic and apparent activation energies as well as pre-exponential factors for the different reaction steps involved. Svelle et al. measured the rates of ethene, propene and *n*-butene methylation with methanol (MeOH) over H-ZSM-5 at high space velocities to minimize by-product formation [13,14]. An increase in alkene size consistently increased the rate and decreased the intrinsic activation energies, being 135, 110 and 90 kJ/mol for ethene, propene and *n*-butene, respectively. The apparent rate constants follow the trends in theoretical studies carried out by means of a small cluster model consisting of four T-atoms [15], and also with *a posteriori* work by Van Speybroeck et al. and Svelle et al. with state of the art computational methods [16,17], reflecting the effect of alkene size in zeolite-catalyzed methylation reactions. A higher methylation rate with increased size and branching of the hydrocarbon molecules has also been found with dimethyl ether

* Corresponding authors.
E-mail address: unni.olsbye@kjemi.uio.no (U. Olsbye).

http://dx.doi.org/10.1016/j.jcat.2017.03.007
0021-9517/

(DME) as methylating agent for H-FER, H-ZSM-5, H-MOR, H-BEA* catalysts [18,19]. Analogous trends have been reported for arene methylation with apparent activation barriers decreasing with the number of methyl substituents connected to the aromatic ring [2,20–23]. For instance, the rate of methylation of benzene, toluene and xylenes over microporous and mesoporous H-ZSM-5 crystals becomes faster for larger arenes. However, xylene rates were strongly influenced by the reaction conditions and this phenomenon was ascribed to possible diffusion limitations or a distinct methylation mechanism at play with respect to benzene and toluene methylation [21]. A diffusion limitation effect has been proposed by Lercher and co-workers who studied toluene, xylene and tri-methylbenzene methylation in large pore-size (H-BEA*, H-MOR) and medium pore-size (H-ZSM-5, H-ZSM-11) zeolites. They suggested that reaction rates can decrease if the size of products is bulky enough to slow down product diffusion as observed in the narrower pores of H-ZSM-5 and H-ZSM-11 [24]. Lesthaege et al. pointed out that the deviations in methylation rate for larger molecules also can be due to a change in the reaction mechanism due to a transition-state-shape selectivity [25].

The effect of zeolite topology during benzene methylation by MeOH was studied in H-ZSM-5 and H-BEA* by Van der Mynsbrugge and co-workers [26]. Two-fold higher methylation rates were observed in H-ZSM-5 compared to H-BEA* zeolite. Theoretical calculations suggest that the stronger stabilization of the transition state is the cause for the higher activity in H-ZSM-5. Van der Mynsbrugge et al. pursued the effects of zeolite topology by studying very distinct zeolites, H-ZSM-58, H-ZSM-22 and H-ZSM-5, as alkene methylation catalysts using DFT methods [27]. They predicted that the methylation rates of ethene, propene and 2-butene were 3 orders of magnitude higher over H-ZSM-5 than over H-ZSM-58 or H-ZSM-22. The high enthalpy barriers in the large cavities of H-ZSM-58 (weak transition-state stabilization) and the high entropic barriers in the narrow channels of H-ZSM-22 (steric hindrance) were reported as responsible for the pronounced differences. The role of acid strength on zeolite-catalyzed methylation reactions has been recently studied by Westgård Erichsen et al. by comparing propene and benzene methylation over highly acidic H-SSZ-24 and weakly acidic H-SAPO-5 [28]. While both hydrocarbons were methylated at similar rates over H-SAPO-5, benzene methylation was significantly faster than propene methylation over H-SSZ-24.

Even though most of the methylation kinetic studies are performed under low conversion levels to minimize by-product formation, the microporous structure and high reactivity of zeolitic materials promote the rapid arousal of secondary reactions. For instance, typical by-products observed during co-reactions of MeOH/DME with benzene or toluene are polymethyl benzenes (polyMBs) and light olefin products, following the dual-cycle mechanism (*i.e.* the mechanism found to dominate the MTH reaction under steady-state conditions, see Scheme 1 [3,24,26,29]). Very recently, the formation of diphenylmethanes (DPMs) has been reported during benzene methylation reactions by MeOH over H-SSZ-24 and H-SAPO-5, although its origin was not identified [28].

The two methylation agents, MeOH and DME, may be interconverted on Brønsted acid sites [31,32] by dehydration of MeOH to form DME and water (Rx. 1). Furthermore, MeOH is formed during methylation of a hydrocarbon by DME (Rx. 2). When MeOH is the methylating agent, a higher hydrocarbon is formed together with water (Rx. 3).

$$2CH_3OH \leftrightarrows CH_3OCH_3 + H_2O \quad (1)$$

$$CH_3OCH_3 + RH \rightarrow RCH_3 + CH_3OH; \qquad RH = \text{alkene, arene} \quad (2)$$

$$CH_3OH + RH \rightarrow RCH_3 + H_2O; \qquad RH = \text{alkene, arene} \quad (3)$$

Only a few studies exist that have compared methylation reactions by MeOH and DME. Apart from one theoretical study by Maihom et al. [33], these studies report DME as more reactive than MeOH over H-ZSM-5 [34,35]. This difference in reactivity is not fully understood yet, as the chemistries of MeOH and DME in zeolite-catalyzed hydrocarbon reactions are closely related. An analogous mechanistic role is generally assumed for MeOH and DME during methylation reactions [33,34,36].Two alternative pathways have been proposed: the concerted and the stepwise mechanisms [2,20,26,37], as shown in Scheme 2. In the concerted mechanism, MeOH or DME react directly with the hydrocarbon in a single step to form a methylated product and H_2O or MeOH respectively. Alternatively, in the stepwise mechanism, MeOH or DME first react unimolecularly on the acid site to form water and a methoxy group. This methoxy group can subsequently act as a methylating agent.

DFT calculations on alkene methylation reactions in H-ZSM-22 have shown that DME stabilizes the methylation transition states to a larger extent than MeOH during a concerted methylation due to an increased entropy effect and additional electrostatic stabilization in comparison to MeOH when the gas phase reactants are the reference state, again leading to faster methylation rates [35]. Regarding the stepwise methylation, the methoxide formation is the distinct step between both oxygenates. Van der Mynsbrugge et al. reported slightly higher free energy barriers for unassisted methoxide formation for MeOH (160 kJ/mol) than for DME (143 kJ/mol) at 397 °C over H-ZSM-5 [38], and this effect might lead to different coverages of methoxy groups when using DME or MeOH. However, the second step of the methylation is identical by reacting methoxide with the alkene/arene. Both mechanisms are assumed to occur during zeolite-catalyzed methylation reactions and the occurrence of one or the other mechanism has been shown to depend on the zeolite topology and reaction conditions. Further work regarding the competition of both mechanisms is found in [20,28,31,35,38].

Apart from the higher methylation activity for DME, a recent contribution regarding the MTH reaction showed a slower catalyst

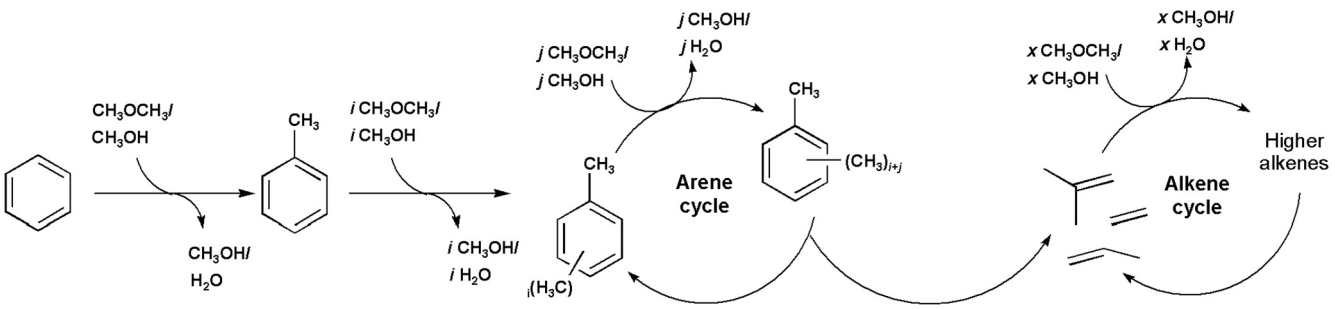

Scheme 1. Expected reactions during co-feed of benzene and MeOH/DME according to the dual-cycle mechanism. Adapted from [28,30].

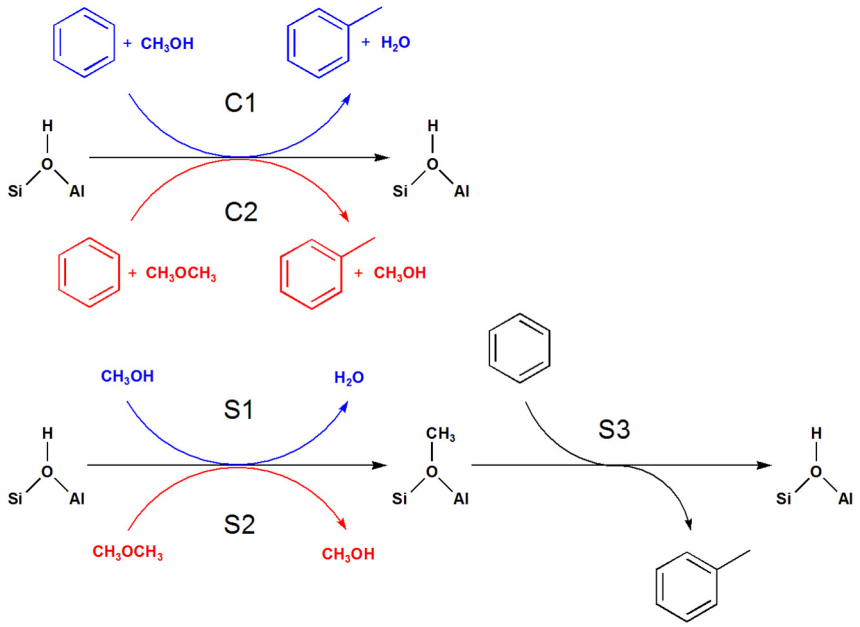

Scheme 2. Representation of the concerted (top) and stepwise (bottom) mechanisms for benzene methylation by means of MeOH (blue) and DME (red).

deactivation rate when using DME as feed instead of MeOH over H-SAPO-34 [39]. Moreover, different intermediates from MeOH and DME have been suggested to be formed during the initial C–C couplings of the MTH reaction [40,41]. It is therefore of interest to compare the reactivity of MeOH and DME in zeolite-catalyzed hydrocarbon conversions, with a focus on a deeper mechanistic understanding of the MTH reaction via isolation of single reactions.

In this work, the reaction of benzene with MeOH and DME is studied over zeolitic materials with different topologies, MFI and AFI, using a combined experimental and computational effort. The first catalyst, H-ZSM-5, is the commercial MTG and MTP catalyst and has an MFI framework characterized by a 3-dimensional pore structure with medium pore size (5.1 × 5.5 Å, 5.3 × 5.6 Å), while the second class of materials has an AFI framework with unidimensional pore structure and large pores (7.3 × 7.3 Å). The large AFI pores facilitate diffusion of polymethylated aromatic compounds. Furthermore, the possibility to synthesize it with a multitude of heteroatoms [42–44] make AFI structured catalysts well suited as model catalysts. In this study, two different AFI compositions were investigated, the aluminosilicate zeolite H-SSZ-24 and the less acidic silicoaluminophosphate zeotype H-SAPO-5. The study revealed novel insight in the reactions occurring between benzene and MeOH or DME. Notably, a parallel pathway to benzene methylation was observed when using methanol (not DME) as the methylating agent, irrespective of the zeolitic catalyst used. The parallel pathway led to diphenylmethane (DPM) formation. Mechanistic details about DPM formation were achieved by an extensive test scheme, mainly using benzene-methanol ($^{12}CH_3OH$, $^{13}CH_3OH$, CD_3OH) co-feed over the H-ZSM-5 catalyst. Furthermore, key reaction steps were subject to static and dynamic DFT calculations. Together, the experimental and theoretical efforts led to a uniform mechanism proposal for DPM formation.

2. Materials and methods

2.1. Catalyst synthesis and characterization

The synthesis of H-SSZ-24 and H-SAPO-5 samples has been described previously [45]. The H-ZSM-5 sample was obtained from ZeoChem. All samples were characterized by powder X-ray diffraction, scanning electron microscopy, microwave plasma Atomic emission spectroscopy (MP-AES), N_2 adsorption, *n*-propylamine TPD [46] and CO-adsorption monitored by FT-Infrared spectroscopy (FTIR). More details on catalyst characterization are available in Supporting Information (Section S1) and in previous works from the group [11,45,47,48]. A brief summary of the catalysts employed is shown in Table 1 below.

2.2. Catalytic testing

Catalytic tests were performed at atmospheric pressure in a fixed bed quartz reactor (inner diameter 8 mm) with catalyst powder pressed and sieved to 250–420 μm. Reaction temperature was monitored by a thermocouple protected by a 3 mm wide quartz sleeve inserted into the middle of the catalyst bed. ^{12}C-MeOH (VWR, 99.8%), ^{13}C-MeOH (Cambridge Isotope Laboratories, 99%), CD_3OH (Sigma–Aldrich, 99%), dimethyl ether (AGA, 25 mol% DME/Argon 6.0), ^{12}C-benzene (Sigma–Aldrich Chroma Solv, 99.9%), ^{12}C-toluene (Sigma–Aldrich Chroma Solv, 99.9%) and distilled water were employed as reactants. The catalysts were activated with an initial heating ramp 5 °C/min under 20% O_2 in helium to 550 °C, and the temperature was kept for 1 h under 100% O_2. Then, the catalysts were cooled to reaction temperature at 5 °C/min under helium flow. Liquid reactants were fed over the catalyst by passing a stream of helium through a flask of boiling reactant. The saturated helium stream was then passed upwards through a water-cooled Vigreux condenser kept at constant temperature (typically 30 °C for MeOH, 35 °C for benzene, 45 °C for toluene, 35 °C for water) by a circulating thermostat water bath. A range of partial pressures and weight hourly space velocities (WHSV) could be obtained by adjusting the flow of either reactant or a third gas line with pure helium.

Benzene co-reaction with MeOH and DME (Section 3.1) was carried out by mixing 5 mg of catalyst powder and 40 mg quartz for H-ZSM-5 and H-SSZ-24, while 40 mg of only catalyst powder was used for H-SAPO-5 due to considerably lower reaction rates obtained over this material. 60 mbar of benzene was co-reacted with 60 mbar of either MeOH or DME at differential conversion (<3%) at 250–300 °C. Additional experiments at 350 °C over H-ZSM-5 gave slightly higher benzene conversion levels (<9%). The experiments were run sequentially by alternating benzene methylation by DME, followed by MeOH and DME again to assure repro-

Table 1
Catalyst properties.

Sample	Structure	Crystal size (μm)	BET surface (m^2/g)	Acid site density (mmol/g)[a]	Si/Al or Al + P/Si[b]	υ(OH) shift (cm^{-1})[c]
H-SAPO-5	AFI	1 × 2	340	0.068	80	−265
H-SSZ-24	AFI	<1	360	0.110	74	−317
H-ZSM-5	MFI	0.5–3	429	0.280	59	−305

[a] Determined via n-propylamine TPD.
[b] Determined via MP-AES.
[c] Determined via FTIR, with CO adsorption.

ducibility and eliminate deactivation effects. The AFI materials were regenerated after every kinetic experiment, while H-ZSM-5 did not require regeneration due to negligible deactivation. Additional Arrhenius-type experiments were run by co-reacting only benzene and MeOH (60:60 mbar) at 250–275–300–325–350 °C over the 3 zeolitic materials.

Co-reaction of benzene and toluene with and without the presence of MeOH, DME and water (Section 3.2) was carried out over 5 mg H-ZSM-5 powder mixed with 40 mg of quartz. The feed composition for most of the co-feed experiments included 60 mbar benzene, 1.5 mbar toluene and 10 mbar oxygenates or water. This feed composition attempted to emulate the composition of the hydrocarbons present during benzene methylation in terms of benzene/toluene ratios when diphenylmethanes were formed. Experiments were carried out at 250 and 300 °C. The same experiments were performed using labeled MeOH and unlabeled benzene and toluene. In this case, the feed composition for most experiments included 60 mbar of benzene, 1.5–3–10 mbar of toluene and 10–15–20 mbar of MeOH. Experiments were carried out at 250, 300 and 350 °C. Also, CD_3OH was co-reacted with benzene under equimolar conditions (60:60 mbar) at 250–350 °C over H-ZSM-5. Partial pressure variation experiments were performed at 250 °C over H-ZSM-5. The partial pressure of either MeOH or benzene was maintained at 60 mbar, while the partial pressure of the other component was varied in the range 10–80 mbar.

The experiments where formaldehyde was formed *in-situ* reported in Section 3.3 were performed by leading a He stream saturated in MeOH through a 1.5 m long stainless steel 1/8″ line heated to 530 °C inspired by the set-up described in [49]. This method allowed the conversion of a maximum of 4% of MeOH fed through the line into methane and formaldehyde. Notably, no reaction between MeOH and formaldehyde with benzene was observed in the absence of catalyst. The catalytic experiments made use of 5 mg H-ZSM-5 diluted with 40 mg quartz. The feed composition for most of the experiments included 60 mbar of benzene and 60 mbar of MeOH:methane:formaldehyde (58:1:1 mbar approximately). Experiments were carried out at 250, 300 and 350 °C.

The effluent from the reactor was analyzed after 10 min of reaction by an on-line GC/MS instrument (Agilent 7890 with flame ionization detector and 5975C MS detector) using two Restek Rtx-DHA-150 columns. In order to track H_2 formation during co-reactions of benzene and MeOH over H-ZSM-5, the effluent was also continuously monitored by on-line MS (Pfeiffer Omnistar) and microGC (Agilent 3000A) with mol sieve column and TC detector.

2.3. Molecular simulations

2.3.1. Static calculations

Periodic Density Functional Theory (DFT) calculations were performed using the Vienna Ab Initio Simulation Package (VASP 5.3) with the PBE functional [50–53]. To account for attractive London dispersion interactions, Grimme's D3 corrections were added [54]. During the calculations, the projector augmented wave (PAW) method was used [55,56], a plane-wave cutoff of 600 eV was adopted and the self-consistent field (SCF) convergence criterion was set to 10^{-5} eV. The Brioullin zone sampling was restricted to the Γ-point.

Transition states were initially optimized with the improved dimer method and then refined with a quasi-Newton algorithm. Geometries were slightly displaced along the normal mode corresponding to the motion that leads the system over the barrier to generate starting geometries for the optimization of reactant and product states. For these calculations a conjugate gradient algorithm was applied.

Static calculations were only performed for the H-ZSM-5 material, using an orthorhombic unit cell consisting of 96 T atoms and one substitutional Al defect and charge compensating proton as Brønsted acid site (Fig. S2). This corresponds to a Si/Al ratio of 95. The Al substitution is located at the T12 position, similar to earlier work [38,57], which is at the intersection of the straight and zigzag channel offering maximum available space and creating the most accessible active site. During all static simulations, the unit cell parameters are kept constant. However, the optimal volume of the unit cell of H-ZSM-5 was calculated by a least square fit to the Birch Murnaghan equation of state curve of the data points depicted in Fig. S3. This led to an optimal unit cell volume of 5467.56 $Å^3$. Subsequently, the unit cell parameters obtained from this structure were used to optimize all configurations with fixed cell parameters: a = 20.02 Å, b = 20.25 Å, c = 13.49 Å, α = 89.87°, β = 89.69°, γ = 90.10°.

For the normal mode analysis (NMA), a partial Hessian vibrational analysis (PHVA) was performed using VASP and our in-house toolkit TAMkin [58]. This means that the guest molecules and an 8T cluster of the framework were taken into account during the NMA, as indicated in Fig. S4. As the potential energy surface (PES) is relatively flat, it can be hard to remove all imaginary frequencies as was also pointed out by De Moor et al. [59] When such superfluous imaginary frequency still appeared after several geometry optimizations with slightly perturbed geometries, this frequency was substituted with an arbitrary value of 50 cm^{-1} as was suggested by De Moor et al.

2.3.2. Molecular dynamics

Ab initio calculations in fully periodic AFI and MFI catalyst models were carried out with the CP2K simulation package (version 2.4) [60,61], using a DFT level of theory with a combination of Gaussian and plane wave basis sets (GPW) [62,63]. For the MD simulations, the revPBE-D3 functional [64] with a DZVP-GTH basis set and pseudopotentials were selected [65]. This combination has been proven successful for applications in zeolite catalysis [66,67].

The AFI materials were represented by a 1 × 1 × 2 super cell consisting of 145 atoms (Fig. S5) and containing one Brønsted acid site. This corresponds to Si/Al and (Al + P)/Si ratios of 47 for H-SSZ-24 and H-SAPO-5, respectively. For the MFI material, the 96T unit cell as described above was applied.

Ab initio molecular dynamics (MD) simulations were performed to assess the adsorption behavior of the guest molecules at realistic reaction temperatures (250 and 350 °C). After an equilibration run of 5 ps, a production run of 50 ps was performed in the NPT ensemble at 1 bar and 350 °C in which the zeolitic framework is

fully flexible. The temperature and pressure were controlled via a chain of 5 Nosé-Hoover thermostats and an MTK barostat, respectively [68,69]. An integration time step of 0.5 fs was applied. Time-averaged cell parameters of the unit and super cells after the NPT simulations are summarized in Table S2.

To calculate the probability that a pre-reactive complex for methylation is formed during an MD simulation of methanol and a co-adsorbed hydrocarbon, the difference between the shortest methanol oxygen – hydrocarbon carbon distance and the shortest methanol carbon - hydrocarbon carbon distance was traced. A sampled state where this difference was higher than 0.5 Å was considered to resemble a pre-reactive complex, as the methyl group pointed toward the benzene molecule. The probability to protonate methanol was computed based on a distance criterion; methanol was considered to be protonated if the distance between the Brønsted acid proton and the methanol oxygen was below 1.2 Å. This procedure has been described elsewhere [28].

3. Results and discussion

3.1. Reactivity of MeOH and DME toward benzene

3.1.1. Experimental assessment

Net product formation rates during benzene methylation by DME and MeOH over H-SAPO-5 and H-SSZ-24 at 250–300 °C, and H-ZSM-5 at 250–350 °C are shown in Fig. 1. Detailed data on the conversion of each reactant are included in Section S3 of the Supporting Information. As can be seen from Fig. 1, there are significant differences in both selectivities and overall activity between the three materials. However, these differences have been the focus of previous contributions (see [28,45,47] for comparisons between the isostructural H-SSZ-24 and H-SAPO-5, and [26] for comparison between two zeolites with different topology, H-ZSM-5 and H-beta) and will not be covered here. Instead, this manuscript will focus on the distinct differences observed between the two methylating reagents.

Concentrating first on the results obtained at 250 °C (Fig. 1, upper panel), two important differences were observed over all catalysts when co-feeding MeOH or DME:

First, the use of DME led to ~5 times, ~3 times and ~6 times faster net formation rate of toluene compared to MeOH under the same contact time conditions, over H-SAPO-5, H-SSZ-24 and H-ZSM-5 respectively. These results are in line with previous studies of H-ZSM-5 at 350 °C, where faster methylation rates of alkenes and methylbenzenes were reported with DME compared to MeOH [34].

Second, and importantly, only three main product groups were observed when using DME as feed: toluene, polyMBs and alkenes, in accordance with the methylation-dealkylation reaction path described in Scheme 1. However, when using MeOH as feed, a fourth abundant product group appeared: Diphenylmethane (DPM) and its methylated analogue, methyldiphenylmethane (Me-DPM). Together, the two products accounted for 13 mol%, 31 mol% and 11 mol% selectivity over H-ZSM-5, H-SSZ-24 and H-SAPO-5, respectively. Conversely, these bulky hydrocarbons were hardly observed in the effluent when DME was used as methylating agent (maximum 2 mol% selectivity over H-SSZ-24). A schematic summary of the group products observed during the co-reaction of benzene with MeOH and DME is presented in Scheme 3.

Experiments performed at 300 °C (Fig. 1, middle panel) mostly reproduced the trends observed at 250 °C. The net formation rates of toluene were ~2, ~4 and ~1.5 times higher over H-ZSM-5, H-SSZ-24 and H-SAPO-5 with DME as methylating agent compared to methanol. Total product formation rates were also faster over the zeolites H-SSZ-24 and H-ZSM-5 when using DME, but a similar total product formation rate with MeOH and DME over H-SAPO-5 was observed at 300 °C. In this latter case, the high conversion of MeOH into DME when co-feeding MeOH and benzene over H-SAPO-5 (almost 50 mol% MeOH converted to DME) complicates the separate assessment of MeOH and DME as methylating agents, in contrast to the two zeolites (Fig. 1, middle right panel). A high activity for methanol dehydration to DME (Rx. 1) over H-SAPO-5 has been reported previously [47]. It was suggested that Rx. (1) is catalyzed by weakly acidic P-OH groups in addition to the more strongly acidic bridge sites in SAPO (and $AlPO_4$) lattices [70]. As observed at 250 °C, significant amounts of DPMs were observed when MeOH was employed, but very small amounts were observed with DME. For all three catalysts, the net formation rate of DPM during methylation with MeOH increased compared to at 250 °C, but less than the increase in methylation rates, leading to an overall decrease in DPM selectivity. The correlation between MeOH versus DME feedstock and DPM selectivity was maintained, but was weaker for H-SAPO-5 than for the two zeolites, in line with the higher DME/MeOH ratio obtained over H-SAPO-5 when feeding MeOH.

Despite the higher conversion levels and the increased prominence of the methanol – DME interconversion reaction (Rx. 1) at 350 °C, significant differences were still observed with respect to primary methylation and competing reactions over H-ZSM-5 (Fig. 1, lower panel). DME remained the more active methylating agent, while MeOH led to 10 times higher net formation rate of DPMs compared to DME.

Together, the data presented in Fig. 1 establish a link between methanol (not DME) and DPM formation. The methanol-DPM route was pursued by temperature variation experiments using a methanol-benzene co-feed.

Fig. 2 shows the temperature dependence of the main product groups observed. Over H-SSZ-24 and H-SAPO-5, all product groups (Toluene, polyMBs, aliphatic products and DPMs) showed exponential temperature dependence at 250–350 °C. The slope of the curve for DPM formation was lower than for the other products. Toluene, polyMBs and aliphatic products showed exponential temperature behavior even over H-ZSM-5, while the production of DPM decreased or stabilized along the temperature range measured. The observed difference between the two topologies could be related to the preferred reaction path over each material, or to a more rapid conversion of DPM to other products in H-ZSM-5 compared to H-SSZ-24 and H-SAPO-5.

3.1.2. Theoretical assessment

In order to rationalize the differences in methylation reactivity between DME and MeOH two sets of calculations were performed. At first instance, we calculated the probability for methanol or DME protonation and the probability to form a pre-reactive complex for a concerted methylation based on the MD runs of methanol or DME with benzene at 250 and 350 °C in H-SAPO-5, H-SSZ-24 and H-ZSM-5. In an earlier study of some of the authors a dynamic tracking of reactivity indices at operating conditions proved successful in explaining the differences in reactivity between H-SAPO-5 and H-SSZ-24 for the benzene methylation [45]. We opted to study the concerted mechanism as at the applied conditions this reaction step was earlier found to be the dominant methylation mechanism [28,71]. The results at both temperatures look very similar and those for 250 °C are displayed in Fig. 3 (results at 350 °C are shown in Fig. S6). A clear clustering of the results per material can be observed. The most striking difference between methanol and DME is observed in the probability to form favorable pre-reactive complexes for benzene methylation. This probability differs by more than a factor 2, indicating a higher intrinsic reactivity of DME than methanol toward methylation. As pointed out in our earlier work, such dynamic analysis correctly accounts for

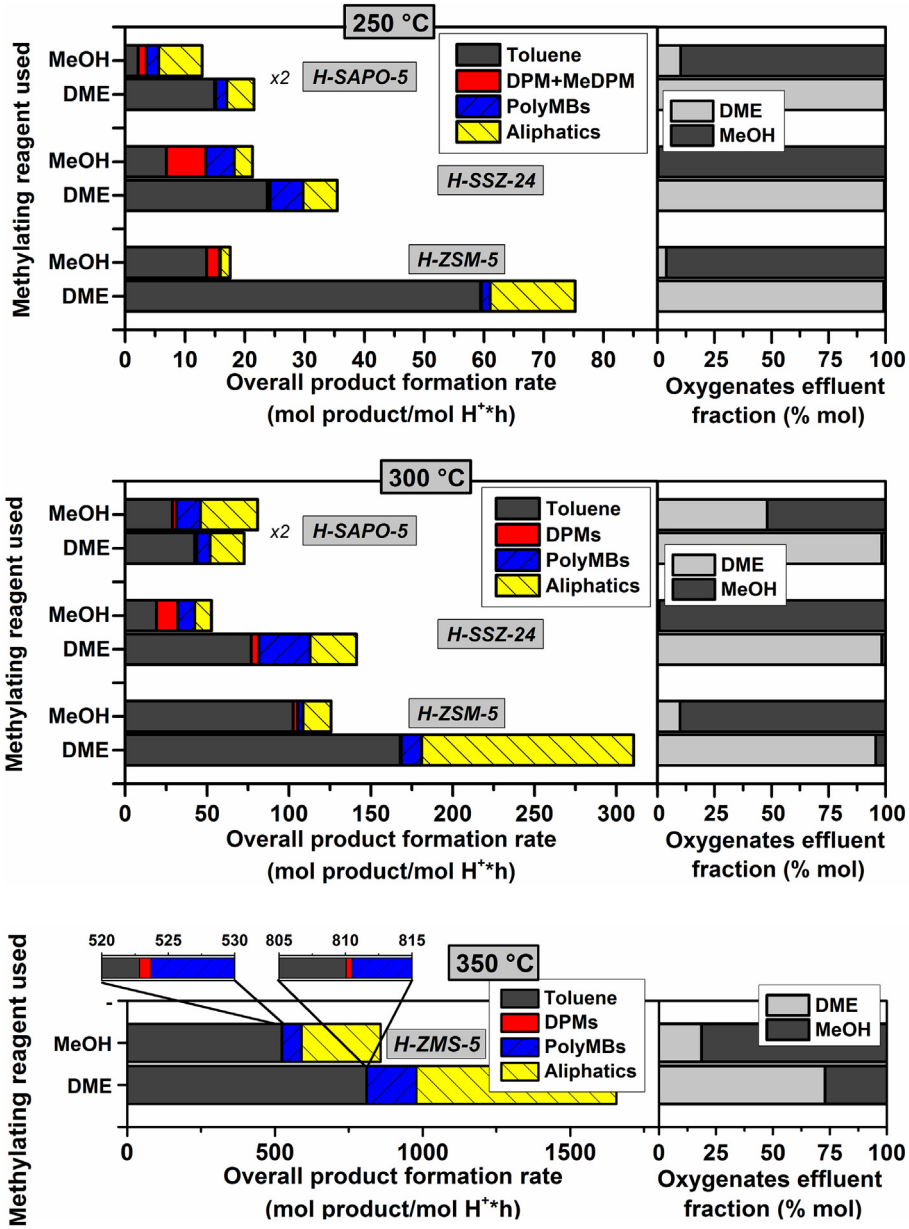

Fig. 1. Net product formation rate (left) and oxygenates effluent fraction (right) during benzene co-reaction with oxygenates (60:60 mbar) over H-SAPO-5, H-SSZ-24 and H-ZSM-5 at 250 °C (top), 300 °C (middle) and 350 °C (only H-ZSM-5, bottom). Total flows = 54.5 mL/min (H-SAPO-5, H-SSZ-24), 100 mL/min (H-ZSM-5), benzene conversion <1% (250 °C), <3% (300 °C), <9% (350 °C). Product formation rates for H-SAPO-5 were multiplied by a factor of 2 for better visualization of the results.

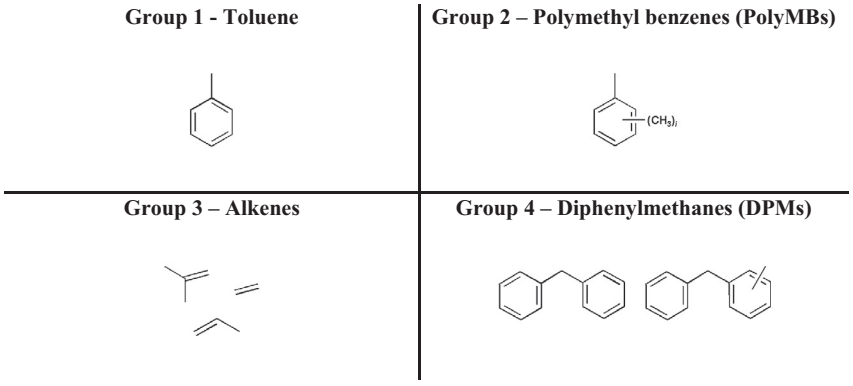

Scheme 3. Summary of the main product groups observed during co-reactions of benzene with MeOH and DME.

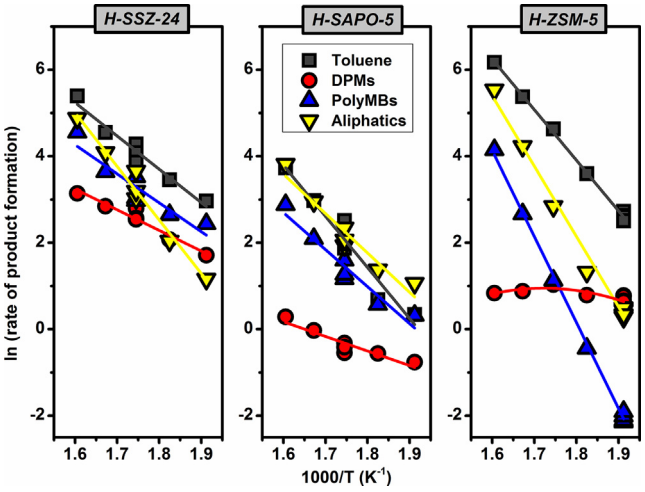

Fig. 2. Temperature correlation for the rate of product formation during the co-feed of benzene:MeOH (60:60 mbar) on H-SSZ-24, H-SAPO-5 and H-ZSM-5 at 250–350 °C. Total flows = 54.5 mL/min (H-SAPO-5, H-SSZ-24), 100 mL/min (H-ZSM-5), benzene conversion <1% (250 °C), <3% (300 °C), <9% (350 °C).

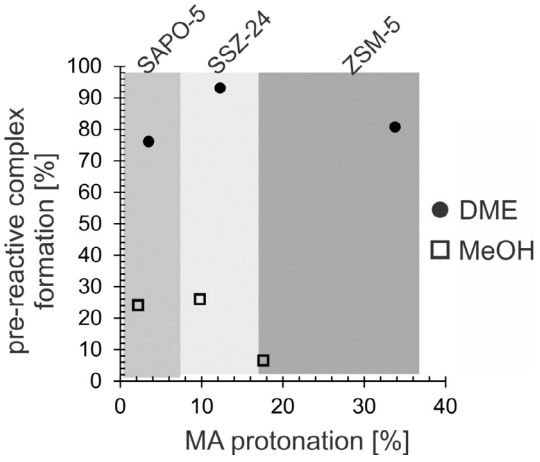

Fig. 3. Probability for methanol or DME protonation (horizontal axis) and probability that a pre-reactive complex is formed (vertical axis) for benzene methylation during 50 ps MD runs of the co-adsorbed complexes in H-SAPO-5, H-SSZ-24 and H-ZSM-5 at 250 °C.

the full configurational freedom of all reactants, as the species are tracked in time at the true operating conditions.

At second instance the benzene methylation rates were explicitly calculated using static DFT calculations in H-ZSM-5. As H-SAPO-5 and H-SSZ-24 are large pore zeolites with substantial configurational freedom, static DFT calculations are less reliable in these materials, since the entropy is not taken into account properly with this approach [67]. Fig. 4 gives the free energy profile obtained for the concerted methylation with DME and MeOH at 250 °C, Table S7 displays the detailed free energy barriers and reaction free energies. When comparing the intrinsic free energy barriers for benzene methylation it seems that DME is slightly more reactive toward benzene methylation than methanol.

3.2. Elucidation of the role of methanol in DPM formation

As DPM and MeDPM (DPMs) were predominantly observed when co-reacting benzene with MeOH and not DME, it is of interest to elucidate what role methanol has in the formation of DPMs. It is possible that methanol is directly involved as reactant, or that either MeOH and/or water, which is not present during reactions with DME, could have an assisting role (analogous to the role played by water and MeOH during polyMB side-chain methylation in SAPO-34 [72]), in the formation of DPMs from toluene and benzene. To distinguish between these possibilities, co-feed studies of benzene and toluene with or without the addition of water, methanol or DME, were carried out over H-ZSM-5 at 250 and 300 °C. The reaction conditions were chosen to emulate conditions where DPM was formed in previous benzene methylation experiments (Section 3.1) with a significant excess of benzene over toluene (60:1.5 mbar). As shown in Fig. 5, no reaction occurred between only benzene and toluene. On the other hand, addition of DME, MeOH and H_2O to the feed promoted the formation of methylated arenes and/or aliphatics from the benzene plus toluene mixture. Importantly, only addition of methanol yielded significant amounts of DPMs. Thus, the possibility for water-assisted direct reactions between toluene and benzene was excluded.

Isotopic distributions observed in DPM and *o*-xylene (as a representative toluene methylation product) after co-reactions of benzene, toluene and ^{13}C-labeled MeOH are shown in Fig. 6. In both molecules, the isotopomer containing one labeled carbon dominated. The fact that DPM dominantly contained one labeled carbon (originating from $^{13}CH_3OH$) clearly demonstrates the direct participation of methanol in DPM formation. The same preference for one labeled carbon atom in DPM (and in *o*-xylene) was observed when varying both MeOH and toluene partial pressures as well as temperature (Fig. S7). These experimental findings clearly indicate that benzene may undergo two parallel reactions when fed together with methanol: A methylation reaction leading to toluene (and to subsequent methylation/dealkylation products), and another reaction in which methanol reacts with two benzene molecules to form DPM (Scheme 4). As no significant reactivity was observed between toluene and benzene, toluene cannot be an intermediate in this latter reaction leading to DPM.

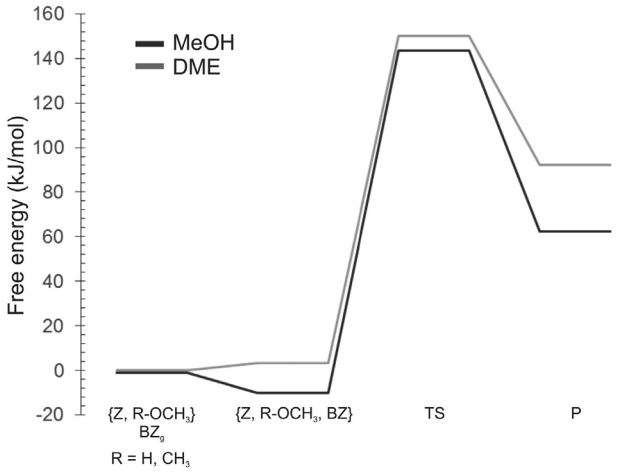

Fig. 4. Free energy diagram for benzene methylation by MeOH or DME in H-ZSM-5 at 250 °C. For the DME transition state an extra imaginary frequency was found that could not be projected out after several geometry perturbations. This frequency was replaced with an arbitrary value of 50 cm^{-1}.

To further assess the reactions involved in toluene and DPM formation, benzene and MeOH partial pressures were systematically varied at the temperature where DPM and toluene formation appear to be more competitive, 250 °C. The results are shown in Fig. 7. Concentrating first on the rate of toluene formation, a positive reaction order in benzene partial pressure is observed. Furthermore, the reaction order in methanol is zero at the lower pressures, and becomes negative at the higher partial pressures of methanol. This result is in agreement with previous literature

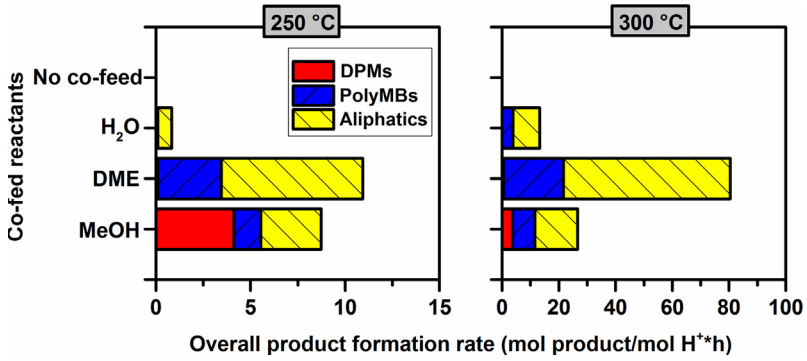

Fig. 5. Net formation of products during toluene phenylation when co-feeding benzene: toluene:MeOH/DME/H_2O (60:1.5:10 mbar) on H-ZSM-5 at 250 °C (left) and 300 °C (right). Total flow = 100 mL/min, benzene conversion <1, 3% at 250 and 300 °C.

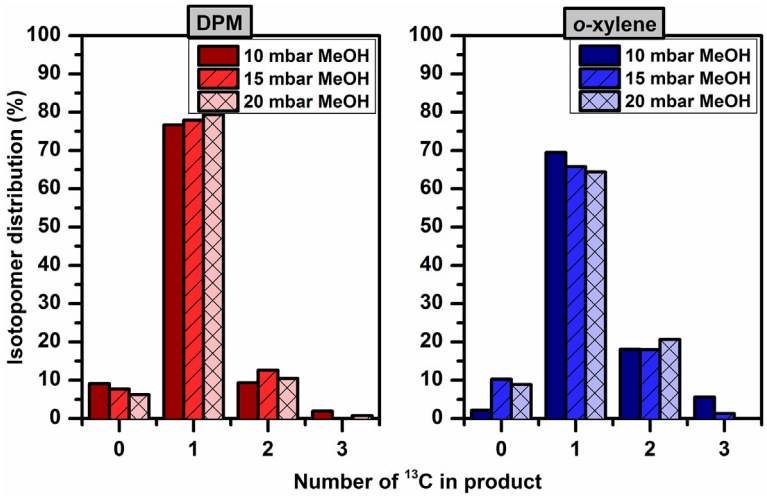

Fig. 6. Isotopomer distribution of DPM (left) and *o*-xylene (right) during co-feed of benzene:toluene:^{13}MeOH (60:1.5:10–20 mbar) over H-ZSM-5 at 250 °C. Total flow = 100 mL/min, benzene conversion <1%.

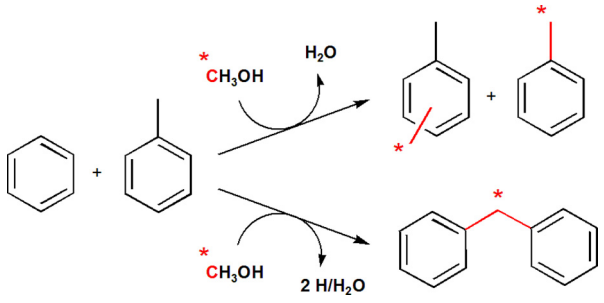

Scheme 4. Proposed competitive reaction pathways during co-feed of benzene, toluene and MeOH: Methylation of arenes to form toluene and xylenes following Scheme 1, and DPM formation via 2 benzene molecules and MeOH condensation with release of 2 hydrogen atoms and water.

on benzene methylation to toluene [21,26], and indicates that the Brønsted acid sites are saturated in methanol under the tested conditions, leading to the reaction path illustrated in Scheme 4 (top pathway). Concentrating next on the DPM formation rate, a positive reaction order is observed in methanol, whereas the reaction order in benzene is negative, in the full range of partial pressures studied. The positive reaction order in methanol could be associated with reaction on a different site or in the gas phase. However, the negative reaction order in benzene for DPM formation, combined with the negative order in methanol for toluene formation at the higher methanol pressures, clearly indicate that the reactions leading to toluene and DPM formation compete for the same active site. Notably, methanol and benzene compete for adsorption on top of the methanol-saturated Brønsted acid site.

Finally, in order to elucidate the type of reaction involved in the rate-determining step of the two competing paths, the co-reaction of benzene with either CH_3OH or CD_3OH was compared over H-ZSM-5 at 250–350 °C. The results are shown in Fig. 8. The rate of toluene formation (left-hand panel) was independent of the methanol isotope used ($k_H/k_D \sim 1$), as expected for a reaction in which C–C bond formation between benzene and a methyl group is the rate-determining step. Conversely, the DPM formation rate (left-hand panel) was consistently reduced along the broad temperature range measured when CD_3OH was used showing a primary kinetic isotope effect with $k_H/k_D \sim 2$. This result is consistent with a reaction in which the rate-determining step involves C-H bond breaking. The isotopomer distribution of DPM at 250 °C (right-hand panel) was shifted by 2 mass units when CD_3OH was used as co-reactant, corroborating the C-H (D) bond rupture in MeOH during the rate determining step to DPM formation.

Together, the results reported in this section strongly suggest that the rate-determining step of DPM formation is dehydrogenation of a methanol molecule on top of a methanol sorbate at the Brønsted acid site.

It has recently been shown that methanol-initiated hydrogen transfer reactions were promoted by Lewis acid sites during the

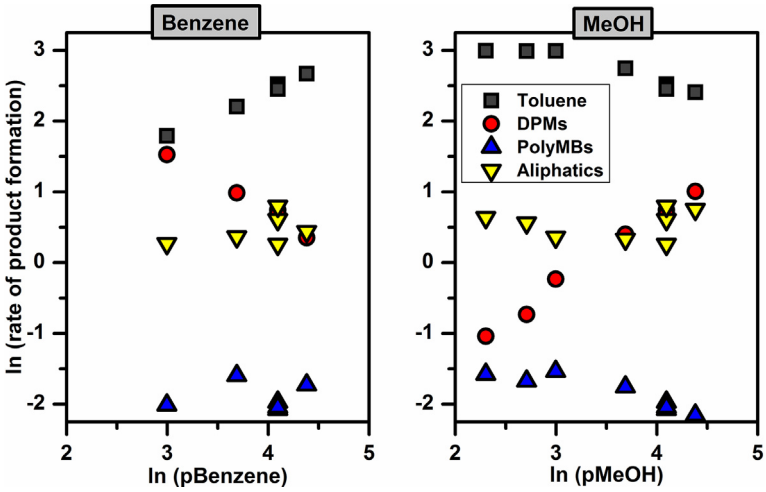

Fig. 7. Net product formation rates variation with benzene (left) and MeOH (right) partial pressures during benzene co-reaction over H-ZSM-5 at 250 °C. Benzene partial pressures were varied in the range 20–80 mbar while keeping MeOH at 60 mbar, while MeOH partial pressures were varied in the range 10–80 mbar, while maintaining benzene at 60 mbar. Total flows = 100 mL/min, benzene conversion <1%.

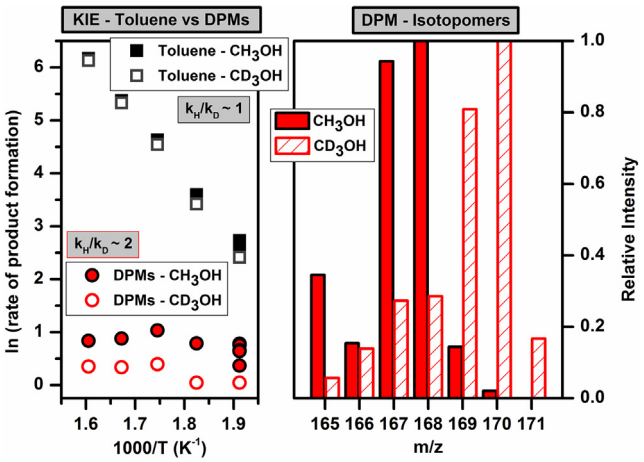

Fig. 8. Temperature correlation for the formation rate of toluene and DPMs at 250-350 °C (left) and DPM isotopomer distribution observed at 250 °C (right) during the co-feed of 60:60 mbar benzene:MeOH (filled symbols) and benzene:MeOH-D3 (empty symbols) on H-ZSM-5. Total flows = 100 mL/min, benzene conversion <9%.

MTH reaction over H-ZSM-5 at 450 °C [73]. In order to further elucidate the contribution of Lewis sites and extra-framework aluminum in methanol dehydrogenation under the conditions used in this study, an H-ZSM-5 sample with similar Brønsted acidity yet distinctively higher Lewis acidity than the sample presented here, was tested for benzene co-reaction with methanol at 250 and 300 °C. The two samples gave similar DPM formation rates at both temperatures (See Supporting Information S4). This result suggests that methanol dehydrogenation primarily occurs on Brønsted acid sites under the conditions studied here.

The results of this section match well with previous literature on the MTH reaction: Several experimental and theoretical studies have suggested that formaldehyde is formed during the initial stages of the MTH reaction, in the so-called methane-formaldehyde mechanism [74–83], as illustrated in Scheme 5.

Importantly, in a very recent contribution, Wei et al. [40] showed theoretically the feasibility to form formaldehyde from MeOH as the most stable species prior to C–C couplings in MTH. On the other hand, DME was found to yield CH_2OCH_3 stable species on the Brønsted sites as the intermediate leading to the first hydrocarbons. The role of the $CH_3OCH_2^+$ cation in the initial C–C bond formation has very recently also been pointed out by Peng et al. using periodic DFT calculations [85]. These results would be in agreement with the deviating behavior of methanol versus DME as methylating agents in the current study.

The reaction shown in Scheme 5 would produce methane as the corresponding reduction product [40,41,74]. Alternatively, the oxidizing agent could be an alkene, in which case a C_{2+} alkane would be formed [4,86–88]. Finally, if no reducing agent is present, then H_2 would be formed [81,89]. The net formation rates of DPM, methane and C_{2+} alkanes over H-ZSM-5 are compared in Table 2. As may be seen, methane was the main reduction product observed, in agreement with Scheme 5, albeit in too low amount to fully account for the DPM formation rate, except at 350 °C. Furthermore, the C_{2+} alkane production was consistently too low to contribute significantly to formaldehyde formation. Finally, no hydrogen was detected by attaching a mass spectrometer and GC with mol sieve column and TC detector to the reactor outlet. However, it should be noted that the sensitivity to hydrogen with our equipment was lower than to hydrocarbons, so this result is not conclusive. The reason for the discrepancy in oxidation and reduction products in the effluent is thus yet to be revealed.

3.3. Formaldehyde reactivity toward benzene

In previous contributions, MeDPM has been observed during toluene transmethylation reactions, and was proposed as an important intermediate in such reactions [90–94]. Furthermore,

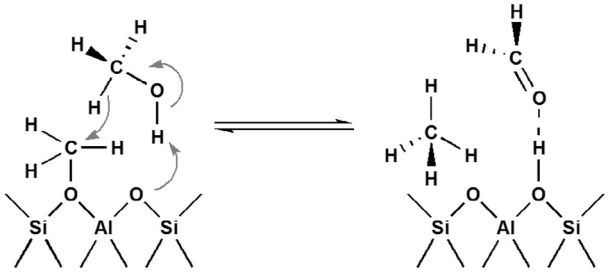

Scheme 5. Representation of the first step proposed to occurred in the methane-formaldehyde mechanism regarding the formation of the first C-C bonds. Adapted from [40,84].

Table 2
Net formation rates of alkanes vs DPM during benzene methylation by MeOH in experiments shown in Fig. 2 for H-ZSM-5.

Sample	Temperature (°C)	DPM formation rate (mol/molH$^+$*h)	Methane formation rate (mol/molH$^+$*h)	Alkanes formation rate (mol/molH$^+$*h)
H-ZSM-5	250	2.2	0.3	b.d.l.
	275	2.4	0.3	b.d.l.
	300	2.8	0.5	b.d.l.
	325	2.4	0.9	0.2
	350	2.3	2.6	1.4

b.d.l. = below detection limit.

the synthesis of diphenylmethane from benzene and formaldehyde over H-ZSM-5 in autoclaves up to 200 °C has been reported [95,96].

To elucidate whether formaldehyde may be involved in the reaction to form DPM under the conditions used in this study, benzene was co-reacted with a MeOH stream containing formaldehyde (58:1:1 mbar MeOH:CH_4:CH_2O). Fig. 9 compares toluene and DPM formation in the absence and presence of formaldehyde, respectively. The addition of formaldehyde led to a decrease of toluene in the effluent, while maintaining the same apparent activation energy for net toluene formation. This result suggests that formaldehyde competes with methanol for adsorption at the Brønsted acid sites, thereby slowing down the methylation reactions. Furthermore, the net DPM formation rate followed an exponential trend with temperature only in the presence of formaldehyde, strongly suggesting that formaldehyde participates in DPM formation.

It is not clear to us why the formaldehyde co-feed did not substantially accelerate DPM formation at the lowest temperature (250 °C). However, it is possible that the rate of coking/polymerization is higher when formaldehyde is present [97]. Finally, the change in temperature dependence of DPM formation with and without formaldehyde co-feed could suggest that the slight decrease in DPM formation from benzene and methanol at 350 °C (without formaldehyde co-feed) is due to slower formaldehyde formation at this temperature.

From static periodic DFT calculations it was also found that formaldehyde exhibits a particularly high reactivity toward reaction with benzene. More specifically, a complete reaction pathway

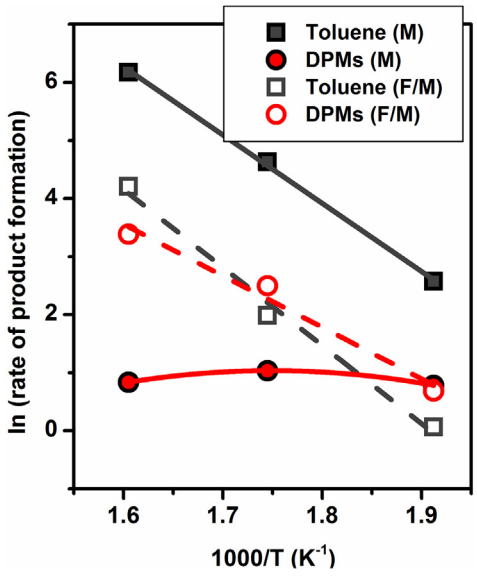

Fig. 9. Arrhenius plot for toluene and diphenylmethane formation when feeding 60 mbar benzene with 60 mbar MeOH and 58:1:1 mbar MeOH:methane:formaldehyde (F/MeOH) in the temperature range 250–350 °C. Total flows = 100 mL/min, benzene conversion <1, 3, 9% at 250, 300 and 350 °C, respectively. Benzene co-reaction with MeOH and F/MeOH are plotted with filled and empty symbols, respectively.

for the formation of DPM starting from formaldehyde and benzene was found. The reaction path and free energy profile at 250 °C are shown in Fig. 10 and the corresponding optimized structures are displayed in Figs. S10 and S11 in the Supporting Information. In a first step, formaldehyde reacts with benzene to form benzyl alcohol. This reaction exhibits a relatively low free energy barrier – around 30–40 kJ/mol lower than the concerted methylation reaction with methanol or DME – indicating the high reactivity of formaldehyde toward benzene. During the optimization of state **2** a quick hydride shift and deprotonation of the post-reactive complex are observed to eventually form physisorbed benzyl alcohol (see Table S10, Fig. S10 and Fig. S11 in the Supporting Information). To accommodate an additional benzene molecule in the MFI channel intersection, the benzyl alcohol molecule needs to reorient, which requires energy. MD simulations at 250 °C confirmed that this reorientation can be assisted by the co-adsorption of the additional benzene molecule (see Supporting Information). As the reorientation of benzyl alcohol upon benzene co-adsorption is a rather dynamic process, our static approach fails to accurately describe the free energy difference between states **2** and **3**. To define this free energy difference, long accelerated MD simulations would be required, which is beyond the scope of this study. It can however be concluded that benzyl alcohol is relatively reactive toward benzene to form DPM, which might explain the absence of benzyl alcohol in the reactor effluent.

Finally, a water molecule and protonated DPM (state 4 in Fig. 10) are formed in a concerted reaction step. The overall free energy barrier for DPM formation starting from formaldehyde and benzene at 250 °C is 152.8 kJ/mol which is in the same order of magnitude as the free energy barriers for methylation (*vide supra*), suggesting that this DPM formation is very likely once formaldehyde has been formed.

It is important to note that our proposed DPM formation pathway requires the presence of formaldehyde, which can presumably only be formed from methanol. It is not clear what role the CH_3-OCH_2^+ cation can play during DPM formation, but as our experimental results clearly show a low DPM selectivity when using a DME feed, it can be expected that it plays a minor role. To further clarify this question, more simulations and experiments would be needed. However, this is beyond the scope of the present study.

The reaction pathway for DPM formation has only been calculated in H-ZSM-5, but a similar mechanism is expected in H-SSZ-24 and H-SAPO-5. Only the rotation (**R**) of the benzylalcohol molecule might be less relevant in the AFI materials due to the large available space in its one-dimensional channels.

4. Conclusions

The reactivity of MeOH and DME toward benzene was thoroughly studied over three different zeolitic catalysts, H-ZSM-5, H-SSZ-24 and H-SAPO-5. DME led to a faster rate of benzene methylation over all materials and under all conditions used in this work. Interestingly, different product selectivity was observed when using DME versus methanol as methylating agent. Whereas DME promoted (successive) methylation of arenes and subsequent dealkylation reactions leading to toluene, polyMB and alkene for-

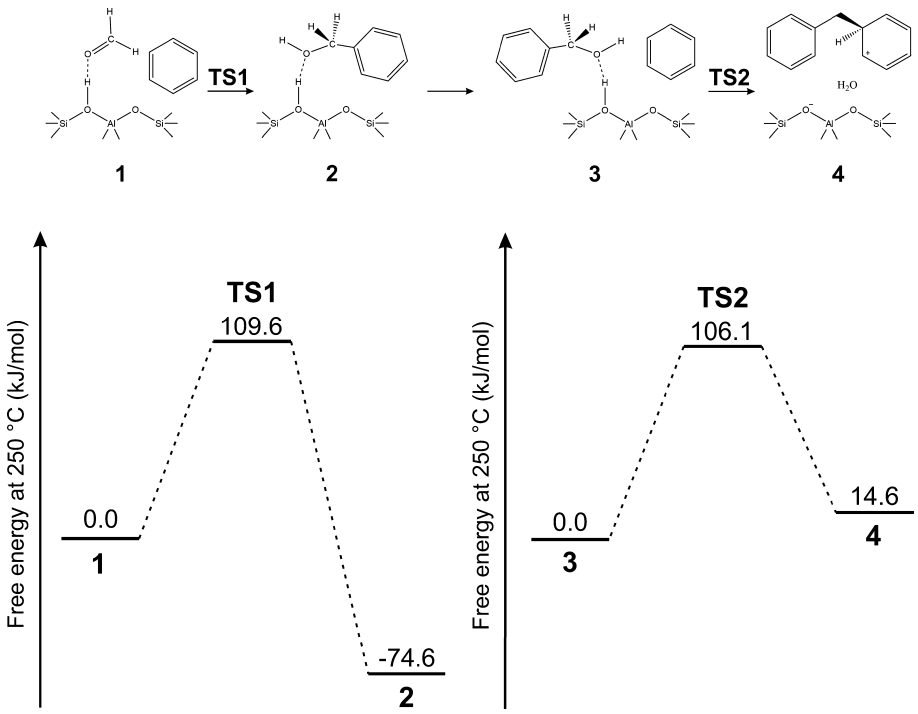

Fig. 10. Reaction scheme and free energy profile for the formation of diphenylmethane in H-ZSM-5 at 250 °C, starting with formaldehyde and benzene.

mation, the use of MeOH formed appreciable amounts of diphenylmethane (DPM) and its methylated analogue in addition to the aforementioned product families. A series of co-reaction experiments involving benzene, toluene and oxygenates or water, as well as ^{13}C- and D_3-labeled methanol, strongly indicated that DPM is formed by methanol dehydrogenation to formaldehyde as the rate-limiting step, followed by reaction with two benzene molecules to form DPM. Partial pressure variation experiments performed over H-ZSM-5 further indicated that the two molecules involved in the rate-limiting step of methylation (benzene) and DPM formation (methanol) compete for the same active site in the catalyst, notably a Brønsted acid site which is saturated in methanol under the test conditions used. A final co-feed experiment over H-ZSM-5, in which formaldehyde was fed with methanol and benzene, confirmed the promoting effect of formaldehyde on DPM formation, as well as a poisoning effect on toluene formation.

DFT calculations encompassing static and molecular dynamics simulations showed that DME exhibits a higher reactivity toward benzene methylation than methanol. This can mainly be ascribed to a dynamical effect in the reactant state which allows DME to form more favorable pre-reactive complexes for the concerted benzene methylation reaction than MeOH. Theory also provided a full pathway for DPM formation starting from formaldehyde and benzene. It could be observed that formaldehyde is highly reactive toward benzene and that the concerted dehydration and carbon-carbon coupling reaction is the rate determining step.

Beyond the reactions studied herein, DPM-like compounds have been previously suggested as coke precursors [98,99]. Furthermore, the use of DME has recently been reported to slow down catalyst deactivation rates compared to MeOH in the conversion of these oxygenates to olefins over H-SAPO-34 [39].

Our study reflects the key role of MeOH in DPM formation over a wide range of temperatures (250–350 °C) and zeolitic catalysts. This study opens the door to a deeper understanding of the complex deactivation puzzle of MTH chemistry, identifying a plausible pathway from MeOH via formaldehyde to coke precursors (MeOH → formaldehyde → DPMs → coke).

Acknowledgements

JSME, SS, TVJ, PB and UO acknowledge the financial support received via the European Industrial Doctorates project "ZeoMorph" (FP7 ITN-EID), part of the Marie Curie actions (grant agreement no-606965).

KDW and VVS acknowledge the Fund for Scientific Research - Flanders (FWO), the Research Board of Ghent University (BOF), BELSPO in the frame of IAP/7/05 funding from the European Union's Horizon 2020 research and innovation programme (consolidator ERC grant agreement No. 647755 – DYNPOR (2015-2020)). The computational resources and services used were provided by Ghent University (Stevin Supercomputer Infrastructure) and the VSC (Flemish Supercomputer Center), funded by the Research Foundation - Flanders (FWO).

Appendix A. Supplementary material

Supplementary data associated with this article can be found, in the online version, at http://dx.doi.org/10.1016/j.jcat.2017.03.007.

References

[1] M.C. Clark, C.M. Smith, D.L. Stern, J.S. Beck, Alkylation of Aromatics, in: Handbook of Heterogeneous Catalysis, Wiley, VCH Verlag GmbH & Co. KGaA, 2008, pp. 3172–3194.
[2] S. Svelle, M. Visur, U. Olsbye, M..Bjørgen. Saepurahman, Mechanistic aspects of the zeolite catalyzed methylation of alkenes and aromatics with methanol: a review, Top. Catal. 54 (2011) 897–906.
[3] U. Olsbye, S. Svelle, M. Bjørgen, P. Beato, T.V.W. Janssens, F. Joensen, S. Bordiga, K.P. Lillerud, Conversion of methanol to hydrocarbons: how zeolite cavity and pore size controls product selectivity, Angew. Chem. Int. Ed. 51 (2012) 5810–5831.
[4] S. Ilias, A. Bhan, Mechanism of the catalytic conversion of methanol to hydrocarbons, ACS Catal. 3 (2013) 18–31.
[5] V. Van Speybroeck, K. De Wispelaere, J. Van Der Mynsbrugge, M. Vandichel, K. Hemelsoet, M. Waroquier, First principle chemical kinetics in zeolites: the

methanol-to-olefin process as a case study, Chem. Soc. Rev. 43 (2014) 7326–7357.
[6] K. Hemelsoet, J. Van Der Mynsbrugge, K. De Wispelaere, M. Waroquier, V. Van Speybroeck, Unraveling the reaction mechanisms governing methanol-to-olefins catalysis by theory and experiment, ChemPhysChem 14 (2013) 1526–1545.
[7] S.M. Csicsery, Shape-selective catalysis in zeolites, Zeolites 4 (1984) 202–213.
[8] J.A. Martens, P.A. Jacobs, Some aspects of molecular shape-selective catalysis with hydrocarbons in zeolites, in: E.G. Derouane, F. Lemos, C. Naccache, F.R. Ribeiro (Eds.), Zeolite Microporous Solids: Synthesis, Structure, and Reactivity, Springer, Netherlands, Dordrecht, 1992, pp. 511–529.
[9] P.B. Venuto, Organic catalysis over zeolites: a perspective on reaction paths within micropores, Microporous Mater. 2 (1994) 297–411.
[10] B. Smit, T.L.M. Maesen, Towards a molecular understanding of shape selectivity, Nature 451 (2008) 671–678.
[11] B.T.L. Bleken, D.S. Wragg, B. Arstad, A.E. Gunnæs, J. Mouzon, S. Helveg, L.F. Lundegaard, P. Beato, S. Bordiga, U. Olsbye, S. Svelle, K.P. Lillerud, Unit cell thick nanosheets of zeolite H-ZSM-5: structure and activity, Top. Catal. 56 (2013) 558–566.
[12] R. Khare, D. Millar, A. Bhan, A mechanistic basis for the effects of crystallite size on light olefin selectivity in methanol-to-hydrocarbons conversion on MFI, J. Catal. 321 (2015) 23–31.
[13] S. Svelle, P.O. Rønning, U. Olsbye, S. Kolboe, Kinetic studies of zeolite-catalyzed methylation reactions. Part 2. Co-reaction of [12C]propene or [12C]n-butene and [13C]methanol, J. Catal. 234 (2005) 385–400.
[14] S. Svelle, P.O. Rønning, S. Kolboe, Kinetic studies of zeolite-catalyzed methylation reactions: 1. Coreaction of [12C]ethene and [13C]methanol, J. Catal. 224 (2004) 115–123.
[15] S. Svelle, B. Arstad, S. Kolboe, O. Swang, A theoretical investigation of the methylation of alkenes with methanol over acidic zeolites, J. Phys. Chem. B 107 (2003) 9281–9289.
[16] V. Van Speybroeck, J. Van der Mynsbrugge, M. Vandichel, K. Hemelsoet, D. Lesthaeghe, A. Ghysels, G.B. Marin, M. Waroquier, First principle kinetic studies of zeolite-catalyzed methylation reactions, J. Am. Chem. Soc. 133 (2011) 888–899.
[17] S. Svelle, C. Tuma, X. Rozanska, T. Kerber, J. Sauer, Quantum chemical modeling of zeolite-catalyzed methylation reactions: toward chemical accuracy for barriers, J. Am. Chem. Soc. 131 (2009) 816–825.
[18] I.M. Hill, S.A. Hashimi, A. Bhan, Kinetics and mechanism of olefin methylation reactions on zeolites, J. Catal. 285 (2012) 115–123.
[19] I.M. Hill, Y.S. Ng, A. Bhan, Kinetics of butene isomer methylation with dimethyl ether over zeolite catalysts, ACS Catal. 2 (2012) 1742–1748.
[20] A.M. Vos, K.H.L. Nulens, F. De Proft, R.A. Schoonheydt, P. Geerlings, Reactivity descriptors and rate constants for electrophilic aromatic substitution: acid zeolite catalyzed methylation of benzene and toluene, J. Phys. Chem. B 106 (2002) 2026–2034.
[21] I. Hill, A. Malek, A. Bhan, Kinetics and mechanism of benzene, toluene, and xylene methylation over H-MFI, ACS Catal. 3 (2013) 1992–2001.
[22] S. Svelle, M. Bjørgen, Mechanistic proposal for the zeolite catalyzed methylation of aromatic compounds, J. Phys. Chem. A 114 (2010) 12548–12554.
[23] V. Van Speybroeck, K. Hemelsoet, K. De Wispelaere, Q. Qian, J. Van der Mynsbrugge, B. De Sterck, B.M. Weckhuysen, M. Waroquier, Mechanistic studies on chabazite-type methanol-to-olefin catalysts: insights from time-resolved UV/Vis microspectroscopy combined with theoretical simulations, ChemCatChem 5 (2013) 173–184.
[24] J.H. Ahn, R. Kolvenbach, S.S. Al-Khattaf, A. Jentys, J.A. Lercher, Methanol usage in toluene methylation with medium and large pore zeolites, ACS Catal. 3 (2013) 817–825.
[25] D. Lesthaeghe, B. De Sterck, V. Van Speybroeck, G.B. Marin, M. Waroquier, Zeolite shape-selectivity in the gem-methylation of aromatic hydrocarbons, Angew. Chem. Int. Ed. 46 (2007) 1311–1314.
[26] J. Van Der Mynsbrugge, M. Visur, U. Olsbye, P. Beato, M. Bjorgen, V. Van Speybroeck, S. Svelle, Methylation of benzene by methanol: single-site kinetics over H-ZSM-5 and H-beta zeolite catalysts, J. Catal. 292 (2012) 201–212.
[27] J. Van der Mynsbrugge, J. De Ridder, K. Hemelsoet, M. Waroquier, V. Van Speybroeck, Enthalpy and entropy barriers explain the effects of topology on the kinetics of zeolite-catalyzed reactions, Chem. – Eur. J. 19 (2013) 11568–11576.
[28] M. Westgård Erichsen, K. De Wispelaere, K. Hemelsoet, S.L.C. Moors, T. Deconinck, M. Waroquier, S. Svelle, V. Van Speybroeck, U. Olsbye, How zeolitic acid strength and composition alter the reactivity of alkenes and aromatics towards methanol Dedicated to the memory of Haldor Topsøe, J. Catal. 328 (2015) 186–196.
[29] J.H. Ahn, R. Kolvenbach, C. Neudeck, S.S. Al-Khattaf, A. Jentys, J.A. Lercher, Tailoring mesoscopically structured H-ZSM5 zeolites for toluene methylation, J. Catal. 311 (2014) 271–280.
[30] M. Westgård Erichsen, J.S. Martinez-Espin, F. Joensen, S. Teketel, P. del Campo Huertas, K.P. Lillerud, S. Svelle, P. Beato, U. Olsbye, Syngas to liquids via oxygenates, in: Small-Scale Gas to Liquid Fuel Synthesis, CRC Press, 2015, pp. 441–474.
[31] A.J. Jones, E. Iglesia, Kinetic, spectroscopic, and theoretical assessment of associative and dissociative methanol dehydration routes in zeolites, Angew. Chem. Int. Ed. 53 (2014) 12177–12181.
[32] C.D. Chang, Hydrocarbons from methanol, Catal. Rev. 25 (1983) 1–118.
[33] T. Maihom, B. Boekfa, J. Sirijaraensre, T. Nanok, M. Probst, J. Limtrakul, Reaction mechanisms of the methylation of ethene with methanol and dimethyl ether over h-zsm-5: an ONIOM study, J. Phys. Chem. C 113 (2009) 6654–6662.
[34] S. Svelle, S. Kolboe, O. Swang, U. Olsbye, Methylation of alkenes and methylbenzenes by dimethyl ether or methanol on acidic zeolites, J. Phys. Chem. B 109 (2005) 12874–12878.
[35] R.Y. Brogaard, R. Henry, Y. Schuurman, A.J. Medford, P.G. Moses, P. Beato, S. Svelle, J.K. Nørskov, U. Olsbye, Methanol-to-hydrocarbons conversion: the alkene methylation pathway, J. Catal. 314 (2014) 159–169.
[36] I.I. Ivanova, A. Corma, Surface species formed and their reactivity during the alkylation of toluene by methanol and dimethyl ether on zeolites as determined by in situ 13C MAS NMR, J. Phys. Chem. B 101 (1997) 547–551.
[37] S.R. Blaszkowski, R.A. Van Santen, Alkylation and transalkylation reactions of aromatics, ACS Symp. Ser. (1999) 307–320.
[38] J. Van Der Mynsbrugge, S.L.C. Moors, K. De Wispelaere, V. Van Speybroeck, Insight into the formation and reactivity of framework-bound methoxide species in h-zsm-5 from static and dynamic molecular simulations, ChemCatChem 6 (2014) 1906–1918.
[39] Y. Li, M. Zhang, D. Wang, F. Wei, Y. Wang, Differences in the methanol-to-olefins reaction catalyzed by SAPO-34 with dimethyl ether as reactant, J. Catal. 311 (2014) 281–287.
[40] Z. Wei, Y. Chen, J. Li, W. Guo, S. Wang, M. Dong, Z. Qin, J. Wang, H. Jiao, W. Fan, Stability and reactivity of intermediates of methanol related reactions and C-C bond formation over H-ZSM-5 ACIDIC CATALYST: A COMPUTATIONAL ANALYSIS, J. Phys. Chem. C 120 (2016) 6075–6087.
[41] Z. Wei, Y.-Y. Chen, J. Li, P. Wang, B. Jing, Y. He, M. Dong, H. Jiao, Z. Qin, J. Wang, W. Fan, Methane formation mechanism in the initial methanol-to-olefins process catalyzed by SAPO-34, Catal. Sci. Technol. 6 (2016) 5526–5533.
[42] E.M. Flanigen, B.M. Lok, R.L. Patton, S.T. Wilson, Aluminophosphate molecular sieves and the periodic table, Stud. Surf. Sci. Catal. (1986) 103–112.
[43] B.M. Weckhuysen, R.R. Rao, J.A. Martens, R.A. Schoonheydt, Transition metal ions in microporous crystalline aluminophosphates: isomorphous substitution, Eur. J. Inorg. Chem. 565–577 (1999).
[44] M. Hartmann, L. Kevan, Transition-metal ions in aluminophosphate and silicoaluminophosphate molecular sieves: location, interaction with adsorbates and catalytic properties, Chem. Rev. 99 (1999) 635–663.
[45] M. Westgård Erichsen, S. Svelle, U. Olsbye, The influence of catalyst acid strength on the methanol to hydrocarbons (MTH) reaction, Catal. Today 215 (2013) 216–223.
[46] C. Pereira, R.J. Gorte, Method for distinguishing Brønsted-acid sites in mixtures of H-ZSM-5, H-Y and silica-alumina, Appl. Catal. A, General 90 (1992) 145–157.
[47] M. Westgård Erichsen, S. Svelle, U. Olsbye, H-SAPO-5 as methanol-to-olefins (MTO) model catalyst: Towards elucidating the effects of acid strength, J. Catal. 298 (2013) 94–101.
[48] F.L. Bleken, K. Barbera, F. Bonino, U. Olsbye, K.P. Lillerud, S. Bordiga, P. Beato, T. V.W. Janssens, S. Svelle, Catalyst deactivation by coke formation in microporous and desilicated zeolite H-ZSM-5 during the conversion of methanol to hydrocarbons, J. Catal. 307 (2013) 62–73.
[49] M.J. Hayman, Modification of methanol-to-olefins hydrocarbon pool species by oxygenates on acidic zeolites, in: University of Southern California, 2011
[50] G. Kresse, J. Furthmüller, Efficient iterative schemes for ab initio total-energy calculations using a plane-wave basis set, Phys. Rev. B – Condensed Matter Mater. Phys. 54 (1996) 11169–11186.
[51] G. Kresse, J. Furthmüller, Efficiency of ab-initio total energy calculations for metals and semiconductors using a plane-wave basis set, Comput. Mater. Sci. 6 (1996) 15–50.
[52] G. Kresse, J. Hafner, Ab initio molecular-dynamics simulation of the liquid-metalamorphous- semiconductor transition in germanium, Phys. Rev. B 49 (1994) 14251–14269.
[53] G. Kresse, J. Hafner, Ab initio molecular dynamics for liquid metals, Phys. Rev. B 47 (1993) 558–561.
[54] S. Grimme, J. Antony, S. Ehrlich, H. Krieg, A consistent and accurate ab initio parametrization of density functional dispersion correction (DFT-D) for the 94 elements H-Pu, J. Chem. Phys. 132 (2010).
[55] P.E. Blöchl, Projector augmented-wave method, Phys. Rev. B 50 (1994) 17953–17979.
[56] G. Kresse, D. Joubert, From ultrasoft pseudopotentials to the projector augmented-wave method, Phys. Rev. B – Condensed Matter Mater. Phys. 59 (1999) 1758–1775.
[57] J. Hajek, J. Van Der Mynsbrugge, K. De Wispelaere, P. Cnudde, L. Vanduyfhuys, M. Waroquier, V. Van Speybroeck, On the stability and nature of adsorbed pentene in Brønsted acid zeolite H-ZSM-5 at 323 K, J. Catal. 340 (2016) 227–235.
[58] A. Ghysels, T. Verstraelen, K. Hemelsoet, M. Waroquier, V. Van Speybroeck, TAMkin: a versatile package for vibrational analysis and chemical kinetics, J. Chem. Inform. Model. 50 (2010) 1736–1750.
[59] B.A. De Moor, M.F. Reyniers, G.B. Marin, Physisorption and chemisorption of alkanes and alkenes in H-FAU: a combined ab initio-statistical thermodynamics study, PCCP 11 (2009) 2939–2958.
[60] J. Vandevondele, M. Krack, F. Mohamed, M. Parrinello, T. Chassaing, J. Hutter, Quickstep: fast and accurate density functional calculations using a mixed Gaussian and plane waves approach, Comput. Phys. Commun. 167 (2005) 103–128.

[61] J. Hutter, M. Iannuzzi, F. Schiffmann, J. Vandevondele, Cp2k: atomistic simulations of condensed matter systems, Wiley Interdisciplinary Rev.: Comput. Mol. Sci. 4 (2014) 15–25.
[62] G. Lippert, J. Hutter, M. Parrinello, The Gaussian and augmented-plane-wave density functional method for ab initio molecular dynamics simulations, Theor. Chem. Acc. 103 (1999) 124–140.
[63] G. Lippert, J. Hutter, M. Parrinello, A hybrid Gaussian and plane wave density functional scheme, Mol. Phys. 92 (1997) 477–487.
[64] K. Yang, J. Zheng, Y. Zhao, D.G. Truhlar, Tests of the RPBE, revPBE, τ -HCTHhyb, ωb97X-D, and MOHLYP density functional approximations and 29 others against representative databases for diverse bond energies and barrier heights in catalysis, J. Chem. Phys. 132 (2010).
[65] S. Goedecker, M. Teter, J. Hutter, Separable dual-space Gaussian pseudopotentials, Phys. Rev. B – Condensed Matter Mater. Phys. 54 (1996) 1703–1710.
[66] S.L.C. Moors, K. De Wispelaere, J. Van Der Mynsbrugge, M. Waroquier, V. Van Speybroeck, Molecular dynamics kinetic study on the zeolite-catalyzed benzene methylation in ZSM-5, ACS Catal. 3 (2013) 2556–2567.
[67] K. Dewispelaere, B. Ensing, A. Ghysels, E.J. Meijer, V. Vanspeybroeck, Complex reaction environments and competing reaction mechanisms in zeolite catalysis: insights from advanced molecular dynamics, Chem. – Eur. J. 21 (2015) 9385–9396.
[68] G.J. Martyna, D.J. Tobias, M.L. Klein, Constant pressure molecular dynamics algorithms, J. Chem. Phys. 101 (1994) 4177–4189.
[69] D. Frenkel, B. Smit, in: Understanding Molecular Simulation, second ed., Academic Press, San Diego, 2002.
[70] W. Dai, W. Kong, G. Wu, N. Li, L. Li, N. Guan, Catalytic dehydration of methanol to dimethyl ether over aluminophosphate and silico-aluminophosphate molecular sieves, Catal. Commun. 12 (2011) 535–538.
[71] K. De Wispelaere, S. Bailleul, V. Van Speybroeck, Towards molecular control of elementary reactions in zeolite catalysis by advanced molecular simulations mimicking operating conditions, Catal. Sci. Technol. 6 (2016) 2686–2705.
[72] K. De Wispelaere, K. Hemelsoet, M. Waroquier, V. Van Speybroeck, Complete low-barrier side-chain route for olefin formation during methanol conversion in H-SAPO-34, J. Catal. 305 (2013) 76–80.
[73] S. Müller, Y. Liu, F.M. Kirchberger, M. Tonigold, M. Sanchez-Sanchez, J.A. Lercher, Hydrogen transfer pathways during zeolite catalyzed methanol conversion to hydrocarbons, J. Am. Chem. Soc. (2016).
[74] G.J. Hutchings, F. Gottschalk, M.V.M. Hall, R. Hunter, Hydrocarbon formation from methylating agents over the zeolite catalyst ZSM-5. Comments on the mechanism of carbon-carbon bond and methane formation, J. Chem. Soc. Faraday Trans. 83 (1987) 571–583.
[75] J. Nováková, L. Kubelková, Z. Dolejšek, Primary reaction steps in the methanol-to-olefin transformation on zeolites, J. Catal. 108 (1987) 208–213.
[76] S.R. Blaszkowski, R.A. Van Santen, Theoretical study of C–C bond formation in the methanol-to- gasoline process, J. Am. Chem. Soc. 119 (1997) 5020–5027.
[77] O. Dewaele, V.L. Geers, G.F. Froment, G.B. Marin, The conversion of methanol to olefins: a transient kinetic study, Chem. Eng. Sci. 54 (1999) 4385–4395.
[78] W. Song, D.M. Marcus, H. Fu, J.O. Ehresmann, J.F. Haw, An oft-studied reaction that may never have been: direct catalytic conversion of methanol or dimethyl ether to hydrocarbons on the solid acids HZSM-5 or HSAPO-34, J. Am. Chem. Soc. 124 (2002) 3844–3845.
[79] D. Lesthaeghe, V. Van Speybroeck, G.B. Marin, M. Waroquier, Understanding the failure of direct C-C coupling in the zeolite-catalyzed methanol-to-olefin process, Angew. Chem. Int. Ed. 45 (2006) 1714–1719.
[80] P. Nachtigall, J. Sauer, Chapter 20 applications of quantum chemical methods in zeolite science, in: J. Čejka, H. van Bekkum, A. Corma, F. Schüth (Eds.), Stud. Surf. Sci. Catal., Elsevier, 2007, pp. 701–XXI.
[81] Y. Liu, S. Müller, D. Berger, J. Jelic, K. Reuter, M. Tonigold, M. Sanchez-Sanchez, J.A. Lercher, Formation mechanism of the first carbon-carbon bond and the first olefin in the methanol conversion into hydrocarbons, Angew. Chem. Int. Ed. 55 (2016) 5723–5726.
[82] L. Kubelková, J. Nováková, K. Nedomová, Reactivity of surface species on zeolites in methanol conversion, J. Catal. 124 (1990) 441–450.
[83] J. Nováková, L. Kubelková, K. Habersberger, Z. Dolejšek, Catalytic activity of dealuminated Y and HZSM-5 zeolites measured by the temperature-programmed desorption of small amounts of preadsorbed methanol and by the low-pressure flow reaction of methanol, J. Chem. Soc. Faraday Trans. 80 (1984) 1457–1465.
[84] S.N. Khadzhiev, M.V. Magomedova, E.G. Peresypkina, Mechanism of olefin synthesis from methanol and dimethyl ether over zeolite catalysts: a review, Petroleum Chem. 54 (2014) 245–269.
[85] C. Peng, H. Wang, P. Hu, Theoretical insights into how the first C–C bond forms in the methanol-to-olefin process catalysed by HSAPO-34, PCCP 18 (2016) 14495–14502.
[86] Z. Wen, T. Xia, M. Liu, K. Zhu, X. Zhu, Methane formation mechanism in methanol to hydrocarbon process: a periodic density functional theory study, Catal. Commun. 75 (2016) 45–49.
[87] Z. Wen, D. Yang, X. He, Y. Li, X. Zhu, Methylation of benzene with methanol over HZSM-11 and HZSM-5: a density functional theory study, J. Mol. Catal. A: Chem.
[88] E.J. Munson, A.A. Kheir, N.D. Lazo, J.F. Haw, In situ solid-state NMR study of methanol-to-gasoline chemistry in zeolite HZSM-5, J. Phys. Chem. 96 (1992) 7740–7746.
[89] S. Senger, L. Radom, Zeolites as transition-metal-free hydrogenation catalysts: a theoretical mechanistic study, J. Am. Chem. Soc. 122 (2000) 2613–2620.
[90] A. Corma, F. Llopis, J.B. Monton, Influence of the structural parameters of Y zeolite on the transalkylation of alkylaromatics, J. Catal. 140 (1993) 384–394.
[91] S. Svelle, U. Olsbye, K.P. Lillerud, S. Kolboe, M. Bjørgen, Diphenylmethane-mediated transmethylation of methylbenzenes over H-zeolites, J. Am. Chem. Soc. 128 (2006) 5618–5619.
[92] M. Guisnet, N.S. Gnep, S. Morin, Mechanisms of xylene isomerization over acidic solid catalysts, Micropor. Mesopor. Mater. 35–36 (2000) 47–59.
[93] Y. Byun, D. Jo, D.N. Shin, S.B. Hong, Theoretical investigation of the isomerization and disproportionation of m-xylene over medium-pore zeolites with different framework topologies, ACS Catal. 4 (2014) 1764–1776.
[94] H.K. Min, S.H. Cha, S.B. Hong, Mechanistic insights into the zeolite-catalyzed isomerization and disproportionation of m -xylene, ACS Catal. 2 (2012) 971–981.
[95] Z. Hou, T. Okuhara, Catalytic synthesis of diphenylmethane from benzene and formalin with water-tolerant solid acids, Appl. Catal.: General 216 (2001) 147–155.
[96] M.J. Climent, A. Corma, H. García, J. Primo, Zeolites in organic reactions condensation of formaldehyde with benzene in the presence of HY zeolites, Appl. Catal. 51 (1989) 113–125.
[97] G.J. Hutchings, L.J. Van Rensburg, W. Pickl, R. Hunter, Hydrocarbon formation from methanol and dimethyl ether using WO_3/Al_2O_3 and H-ZSM-5 catalysts. A mechanistic investigation using model reagents, J. Chem. Soc. Faraday Trans. 84 (1988) 1311–1328.
[98] M. Guisnet, P. Magnoux, Organic chemistry of coke formation, Appl. Catal.: General 212 (2001) 83–96.
[99] S. Morin, N.S. Gnep, M. Guisnet, Influence of coke deposits on the selectivity of m-xylene transformation and on the isomerization mechanism, Appl. Catal.: General 168 (1998) 63–68.